

# First observation of $J/\psi$ and $\psi(2S)$ decaying to $nK_S^0\bar{\Lambda} + c.c.$

M. Ablikim<sup>1</sup>, J. Z. Bai<sup>1</sup>, Y. Ban<sup>13</sup>, X. Cai<sup>1</sup>, H. F. Chen<sup>18</sup>, H. S. Chen<sup>1</sup>, H. X. Chen<sup>1</sup>, J. C. Chen<sup>1</sup>, Jin Chen<sup>1</sup>, Y. B. Chen<sup>1</sup>, Y. P. Chu<sup>1</sup>, Y. S. Dai<sup>20</sup>, L. Y. Diao<sup>10</sup>, Z. Y. Deng<sup>1</sup>, Q. F. Dong<sup>16</sup>, S. X. Du<sup>1</sup>, J. Fang<sup>1</sup>, S. S. Fang<sup>1a</sup>, C. D. Fu<sup>16</sup>, C. S. Gao<sup>1</sup>, Y. N. Gao<sup>16</sup>, K. Götzen<sup>3</sup>, S. D. Gu<sup>1</sup>, Y. T. Gu<sup>5</sup>, Y. N. Guo<sup>1</sup>, Z. J. Guo<sup>17b</sup>, F. A. Harris<sup>17</sup>, K. L. He<sup>1</sup>, M. He<sup>14</sup>, Y. K. Heng<sup>1</sup>, J. Hou<sup>12</sup>, H. M. Hu<sup>1</sup>, J. H. Hu<sup>4</sup>, T. Hu<sup>1</sup>, G. S. Huang<sup>1c</sup>, X. T. Huang<sup>14</sup>, X. B. Ji<sup>1</sup>, X. S. Jiang<sup>1</sup>, X. Y. Jiang<sup>6</sup>, J. B. Jiao<sup>14</sup>, D. P. Jin<sup>1</sup>, S. Jin<sup>1</sup>, Y. F. Lai<sup>1</sup>, G. Li<sup>1d</sup>, H. B. Li<sup>1</sup>, J. Li<sup>1</sup>, R. Y. Li<sup>1</sup>, S. M. Li<sup>1</sup>, W. D. Li<sup>1</sup>, W. G. Li<sup>1</sup>, X. L. Li<sup>1</sup>, X. N. Li<sup>1</sup>, X. Q. Li<sup>12</sup>, Y. F. Liang<sup>15</sup>, H. B. Liao<sup>1</sup>, B. J. Liu<sup>1</sup>, C. X. Liu<sup>1</sup>, F. Liu<sup>7</sup>, Fang Liu<sup>1</sup>, H. H. Liu<sup>1</sup>, H. M. Liu<sup>1</sup>, J. Liu<sup>13e</sup>, J. B. Liu<sup>1</sup>, J. P. Liu<sup>19</sup>, Jian Liu<sup>1</sup>, Q. Liu<sup>17</sup>, R. G. Liu<sup>1</sup>, Z. A. Liu<sup>1</sup>, Y. C. Lou<sup>6</sup>, F. Lu<sup>1</sup>, G. R. Lu<sup>6</sup>, J. G. Lu<sup>1</sup>, C. L. Luo<sup>11</sup>, F. C. Ma<sup>10</sup>, H. L. Ma<sup>2</sup>, L. L. Ma<sup>1f</sup>, Q. M. Ma<sup>1</sup>, Z. P. Mao<sup>1</sup>, X. H. Mo<sup>1</sup>, J. Nie<sup>1</sup>, S. L. Olsen<sup>17</sup>, K. J. Peters<sup>3</sup>, R. G. Ping<sup>1</sup>, N. D. Qi<sup>1</sup>, H. Qin<sup>1</sup>, J. F. Qiu<sup>1</sup>, Z. Y. Ren<sup>1</sup>, G. Rong<sup>1</sup>, X. D. Ruan<sup>5</sup>, L. Y. Shan<sup>1</sup>, L. Shang<sup>1</sup>, C. P. Shen<sup>17</sup>, D. L. Shen<sup>1</sup>, X. Y. Shen<sup>1</sup>, H. Y. Sheng<sup>1</sup>, H. S. Sun<sup>1</sup>, S. S. Sun<sup>1</sup>, Y. Z. Sun<sup>1</sup>, Z. J. Sun<sup>1</sup>, X. Tang<sup>1</sup>, G. L. Tong<sup>1</sup>, G. S. Varner<sup>17</sup>, D. Y. Wang<sup>1g</sup>, L. Wang<sup>1</sup>, L. L. Wang<sup>1</sup>, L. S. Wang<sup>1</sup>, M. Wang<sup>1</sup>, P. Wang<sup>1</sup>, P. L. Wang<sup>1</sup>, W. F. Wang<sup>1h</sup>, Y. F. Wang<sup>1</sup>, Z. Wang<sup>1</sup>, Z. Y. Wang<sup>1</sup>, Zheng Wang<sup>1</sup>, C. L. Wei<sup>1</sup>, D. H. Wei<sup>4</sup>, Y. Weng<sup>1</sup>, N. Wu<sup>1</sup>, X. M. Xia<sup>1</sup>, X. X. Xie<sup>1</sup>, G. F. Xu<sup>1</sup>, X. P. Xu<sup>7</sup>, Y. Xu<sup>12</sup>, M. L. Yan<sup>18</sup>, H. X. Yang<sup>1</sup>, Y. X. Yang<sup>4</sup>, M. H. Ye<sup>2</sup>, Y. X. Ye<sup>18</sup>, G. W. Yu<sup>1</sup>, C. Z. Yuan<sup>1</sup>, Y. Yuan<sup>1</sup>, S. L. Zang<sup>1</sup>, Y. Zeng<sup>8</sup>, B. X. Zhang<sup>1</sup>, B. Y. Zhang<sup>1</sup>, C. C. Zhang<sup>1</sup>, D. H. Zhang<sup>1</sup>, H. Q. Zhang<sup>1</sup>, H. Y. Zhang<sup>1</sup>, J. W. Zhang<sup>1</sup>, J. Y. Zhang<sup>1</sup>, S. H. Zhang<sup>1</sup>, X. Y. Zhang<sup>14</sup>, Yiyun Zhang<sup>15</sup>, Z. X. Zhang<sup>13</sup>, Z. P. Zhang<sup>18</sup>, D. X. Zhao<sup>1</sup>, J. W. Zhao<sup>1</sup>, M. G. Zhao<sup>1</sup>, P. P. Zhao<sup>1</sup>, W. R. Zhao<sup>1</sup>, Z. G. Zhao<sup>1i</sup>, H. Q. Zheng<sup>13</sup>, J. P. Zheng<sup>1</sup>, Z. P. Zheng<sup>1</sup>, L. Zhou<sup>1</sup>, K. J. Zhu<sup>1</sup>, Q. M. Zhu<sup>1</sup>, Y. C. Zhu<sup>1</sup>, Y. S. Zhu<sup>1</sup>, Z. A. Zhu<sup>1</sup>, B. A. Zhuang<sup>1</sup>, X. A. Zhuang<sup>1</sup>, B. S. Zou<sup>1</sup>.

(BES Collaboration)

<sup>1</sup> Institute of High Energy Physics, Beijing 100049, People's Republic of China

<sup>2</sup> China Center for Advanced Science and Technology (CCAST), Beijing 100080, People's Republic of China

<sup>3</sup> GSI mbh Darmstadt, Darmstadt, 64291, Germany

<sup>4</sup> Guangxi Normal University, Guilin 541004, People's Republic of China

<sup>5</sup> Guangxi University, Nanning 530004, People's Republic of China

<sup>6</sup> Henan Normal University, Xinxiang 453002, People's Republic of China

<sup>7</sup> Huazhong Normal University, Wuhan 430079, People's Republic of China

<sup>8</sup> Hunan University, Changsha 410082, People's Republic of China

<sup>9</sup> Jinan University, Jinan 250022, People's Republic of China

<sup>10</sup> Liaoning University, Shenyang 110036, People's Republic of China

<sup>11</sup> Nanjing Normal University, Nanjing 210097, People's Republic of China

<sup>12</sup> Nankai University, Tianjin 300071, People's Republic of China

<sup>13</sup> Peking University, Beijing 100871, People's Republic of China

<sup>14</sup> Shandong University, Jinan 250100, People's Republic of China

<sup>15</sup> Sichuan University, Chengdu 610064, People's Republic of China

<sup>16</sup> Tsinghua University, Beijing 100084, People's Republic of China

<sup>17</sup> University of Hawaii, Honolulu, HI 96822, USA

<sup>18</sup> University of Science and Technology of China, Hefei 230026, People's Republic of China

<sup>19</sup> Wuhan University, Wuhan 430072, People's Republic of China

<sup>20</sup> Zhejiang University, Hangzhou 310028, People's Republic of China

<sup>a</sup> Current address: DESY, D-22607, Hamburg, Germany

<sup>b</sup> Current address: Johns Hopkins University, Baltimore, MD 21218, USA

<sup>c</sup> Current address: University of Oklahoma, Norman, OK 73019, USA

<sup>d</sup> Current address: Universite Paris XI, LAL-Bat. 208-BP34, 91898 ORSAY Cedex, France

<sup>e</sup> Current address: Max-Planck-Institut fuer Physik, Foehringer Ring 6, 80805 Munich, Germany

<sup>f</sup> Current address: University of Toronto, Toronto M5S 1A7, Canada

<sup>g</sup> Current address: CERN, CH-1211 Geneva 23, Switzerland

<sup>h</sup> Current address: Laboratoire de l'Accélérateur Linéaire, Orsay, F-91898, France

<sup>i</sup> Current address: University of Michigan, Ann Arbor, MI 48109, USA

The decays of  $J/\psi$  and  $\psi(2S)$  to  $nK_S^0\bar{\Lambda} + c.c.$  are observed and measured for the first time, and the perturbative QCD prediction is compared with the experimental results. The branching fractions are  $\mathcal{B}(J/\psi \rightarrow nK_S^0\bar{\Lambda} + c.c.) = (1.1 \pm 0.2) \times 10^{-4}$  and  $\mathcal{B}(\psi(2S) \rightarrow nK_S^0\bar{\Lambda} + c.c.) = (1.1 \pm 0.2) \times 10^{-4}$ .

## 1. Introduction

Since the discovery of the  $J/\psi$  at Brookhaven [1] and SLAC [2] in 1974, more than one hundred exclusive decay modes of the  $J/\psi$  have been reported. According to Ref. [3], direct hadronic, electromagnetic and radiative decays make up roughly 65%, 14%, and 7% of the total  $J/\psi$  decay width, respectively. However, the measured hadronic decay channels sum up to less than 35 %. The BESII data sample of  $5.8 \times 10^7$   $J/\psi$  events provides a good opportunity to search for missing  $J/\psi$  hadronic decays.

In 2004, BESII reported the observation of an enhancement  $X(2075)$  near the threshold of the invariant mass spectrum of  $p\bar{\Lambda}$  in  $J/\psi \rightarrow pK^-\bar{\Lambda}$  decays. The mass, width, and product branching fraction of this enhancement are  $M = 2075 \pm 12$  (stat.)  $\pm 5$  (syst.) MeV/ $c^2$ ,  $\Gamma = 90 \pm 35$  (stat.)  $\pm 9$  (syst.) MeV/ $c^2$  [4], and  $B(J/\psi \rightarrow K^-X)B(X \rightarrow p\bar{\Lambda} + c.c.) = (5.9 \pm 1.4 \pm 2.0) \times 10^{-5}$ , respectively. The study of the isospin conjugate channel  $J/\psi \rightarrow nK_S^0\bar{\Lambda}$  is therefore important not only in exploring new decay modes of  $J/\psi$  but also in understanding the  $X(2075)$ .

The  $5.8 \times 10^7$   $J/\psi$  and  $1.4 \times 10^7$   $\psi(2S)$  events at BESII also offer a unique opportunity to search for new decay modes of  $J/\psi$  and  $\psi(2S)$  and test the “12% rule” in hadronic decays. In perturbative QCD, hadronic decays of the  $J/\psi$  and  $\psi(2S)$  are expected to proceed dominantly via three gluons or a single direct photon with widths proportional to the square of the  $c\bar{c}$  wave function at the origin, which is well determined from dilepton decays. Thus for any hadronic final state  $h$ , the  $J/\psi$  and  $\psi(2S)$  decay branching fractions should satisfy the so called “12% rule” [5].

$$Q_h = \frac{B(\psi(2S) \rightarrow h)}{B(J/\psi \rightarrow h)} \simeq \frac{B(\psi(2S) \rightarrow e^+e^-)}{B(J/\psi \rightarrow e^+e^-)} \simeq 12\%.$$

The leptonic branching fractions are taken from the particle data group (PDG) [6] tables. It is roughly obeyed for a number of exclusive hadronic decay channels except some  $VP$ ,  $PP$  and  $VT$  channels [7][8][9], where  $P, V$  and  $T$  denote members of the pseudoscalar, vector and tensor nonets, respectively.

In this paper, the first observation and mea-

surement of  $J/\psi$  and  $\psi(2S)$  to  $nK_S^0\bar{\Lambda} + c.c.$ , as well as a test of the perturbative QCD 12% rule are presented. The  $\Lambda^*$  and  $N^*$  resonance structures in  $J/\psi \rightarrow nK_S^0\bar{\Lambda} + c.c.$  are also shown, where no obvious enhancement near  $n\bar{\Lambda}$  threshold is observed. The upper limit on the branching fraction of  $J/\psi \rightarrow K_S^0X, X \rightarrow n\bar{\Lambda}$  is determined.

## 2. The BES Detector

The upgraded Beijing Spectrometer detector (BESII) is located at the Beijing Electron-Positron Collider (BEPC). BESII is a large solid-angle magnetic spectrometer which is described in detail in Ref. [10]. The momentum of charged particles is determined by a 40-layer cylindrical main drift chamber (MDC) which has a momentum resolution of  $\sigma_p/p = 1.78\% \sqrt{1 + p^2}$  ( $p$  in GeV/ $c$ ). Particle identification is accomplished using specific ionization ( $dE/dx$ ) measurements in the drift chamber and time-of-flight (TOF) information in a barrel-like array of 48 scintillation counters. The  $dE/dx$  resolution is  $\sigma_{dE/dx} \simeq 8.0\%$ ; the TOF resolution for Bhabha events is  $\sigma_{TOF} = 180$  ps. Radially outside of the time-of-flight counters is a 12-radiation-length barrel shower counter (BSC) comprised of gas tubes interleaved with lead sheets. The BSC measures the energy and direction of photons with resolutions of  $\sigma_E/E \simeq 21\% \sqrt{E}$  ( $E$  in GeV),  $\sigma_\phi = 7.9$  mrad, and  $\sigma_z = 2.3$  cm. The iron flux return of the magnet is instrumented with three double layers of proportional counters that are used to identify muons.

A GEANT3 based Monte Carlo (MC) program (SIMBES) [11] with detailed consideration of the detector performance is used. The consistency between data and MC has been carefully checked in many high purity physics channels, and the agreement is reasonable. More details on this comparison can be found in Ref. [11]. The detection efficiency and mass resolution for each decay mode in this analysis are obtained from MC simulation.

### 3. Analysis

The analyzed  $J/\psi$  and  $\psi(2S) \rightarrow nK_S^0\bar{\Lambda}$  with  $K_S^0 \rightarrow \pi^+\pi^-$  and  $\bar{\Lambda} \rightarrow \bar{p}\pi^+$  (and *c.c.*) final states contain four charged tracks and an undetected neutron or anti-neutron. We require the candidate events to satisfy the following common selection criteria:

1. Events must have four good charged tracks with zero net charge. A good charged track is a track that is well fitted to a three-dimensional helix, originates from the interaction region and has a polar angle  $\theta$  in the range  $|\cos\theta| < 0.8$ . Because of the long decay lengths before  $K_S^0$  and  $\bar{\Lambda}$  decay to  $\pi^+\pi^-$  and  $\bar{p}\pi^+$ , the interaction region is defined as  $R_{xy} < 0.12$  m and  $|z| < 0.3$  m. Here,  $R_{xy}$  is the distance from the beamline to the point of closest approach of the track to the beamline, and  $|z|$  is the distance along the beamline to this point from the interaction point.
2. For each charged track in an event,  $\chi_{PID}^2(i)$  is determined using both  $dE/dx$  and TOF information:

$$\chi_{PID}^2(i) = \chi_{dE/dx}^2(i) + \chi_{TOF}^2(i),$$

where  $i$  corresponds to the particle hypothesis. A charged track is identified as a  $p$  if  $\chi_{PID}^2$  for the  $p$  hypothesis is less than those for the  $\pi$  or  $K$  hypotheses. For the channels studied, one charged track must be identified as a  $p$  or  $\bar{p}$ .

#### 3.1. Measurement of $J/\psi \rightarrow nK_S^0\bar{\Lambda} + c.c.$

For  $J/\psi \rightarrow nK_S^0\bar{\Lambda} \rightarrow \bar{p}n\pi^+\pi^-\pi^+$ , the  $K_S^0 \rightarrow \pi^+\pi^-$  and  $\bar{\Lambda} \rightarrow \bar{p}\pi^+$  decays are reconstructed using secondary vertex fitting, and the  $\pi^+$  from the  $\bar{\Lambda}$  decay is identified. To select  $\Lambda(\bar{\Lambda})$  [ $\Lambda(\bar{\Lambda})$  mass selection],  $|M_{p\pi^-}(\bar{p}\pi^+) - 1.115| < 0.012$  GeV/ $c^2$  is required, and to select  $K_S^0$  ( $K_S^0$  mass selection),  $|M_{\pi^+\pi^-} - 0.497| < 0.02$  GeV/ $c^2$  is required. To reject the backgrounds from channels containing a  $K_S^0$  but no  $\Lambda$ , like e.g.  $J/\psi \rightarrow \bar{p}K_S^0\Sigma^- + c.c.$ , we require  $L_{xy}(\Lambda)$ , the distance from the reconstructed  $\Lambda$  vertex to the event origin, to be larger than 5 mm.

Figure 1 is the missing mass spectrum determined from the charged tracks in  $J/\psi \rightarrow nK_S^0\bar{\Lambda} + c.c.$  candidate events satisfying  $\Lambda(\bar{\Lambda})$  and  $K_S^0$  mass selections and  $L_{xy}(\Lambda) > 5$  mm. A clear peak at the nominal neutron mass is observed. The second peak in the high missing mass region comes from  $J/\psi \rightarrow nK_S^0\bar{\Sigma}^0(1385) + c.c.$  and  $J/\psi \rightarrow \Sigma^-\bar{\Sigma}^+(1385) + c.c.$  backgrounds. To suppress background and improve the resolution, a one constraint (1C) kinematic fit with a missing neutron is applied under the  $J/\psi \rightarrow \bar{p}n\pi^+\pi^-\pi^+$  hypothesis. The distribution of 1C fit  $\chi_{\bar{p}n\pi^+\pi^-\pi^+}^2$  for the above selection is shown in Fig. 2. The agreement between data and MC simulation is reasonable, and in the following,  $\chi_{1C}^2 < 5$  is required.

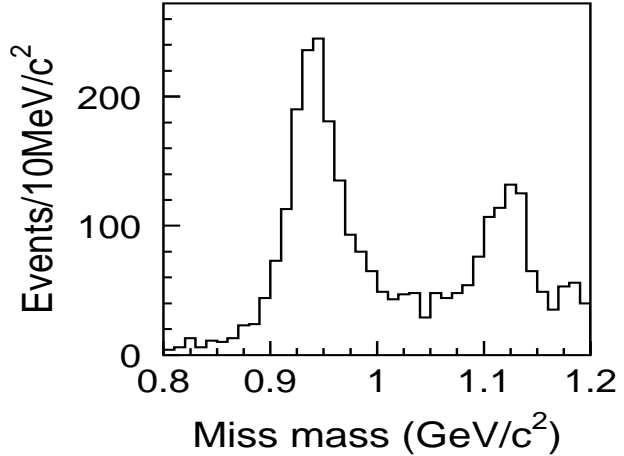


Figure 1. The missing mass determined from the charged tracks in  $J/\psi \rightarrow nK_S^0\bar{\Lambda} + c.c.$  candidate events satisfying  $\Lambda(\bar{\Lambda})$  and  $K_S^0$  mass selections and  $L_{xy}(\Lambda) > 5$  mm.

Figure 3 shows the scatter plot of  $m_{\bar{p}\pi^+}$  versus  $m_{\pi^+\pi^-}$ , and clear  $\bar{\Lambda}$  and  $K_S^0$  signals are seen. Figure 4 shows the  $\Lambda$  decay length distributions for data and MC simulation for events satisfying  $\Lambda(\bar{\Lambda})$  and  $K_S^0$  mass selection requirements and  $\chi_{1C}^2 < 5$ . The missing mass distribution

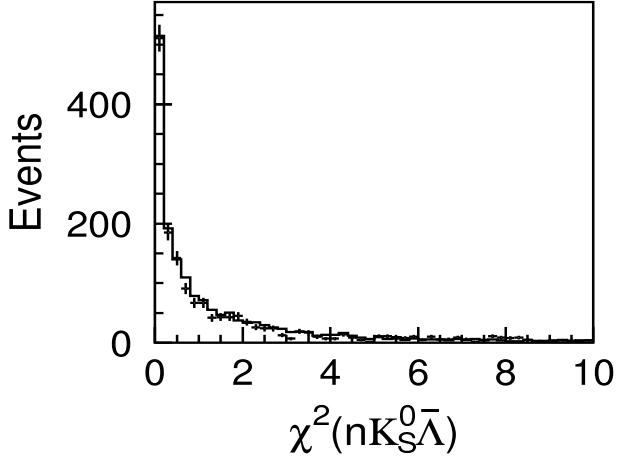


Figure 2. The  $\chi^2$  distributions for the 1C fits to the  $J/\psi \rightarrow \bar{p}n\pi^+\pi^-\pi^+$  hypothesis for  $J/\psi \rightarrow nK_S^0\bar{\Lambda}$  candidate events for the selection used in Fig 1. The crosses are data; the full histograms are the sum of MC simulation of  $J/\psi \rightarrow nK_S^0\bar{\Lambda}$  and background determined from  $K_S^0$  sidebands ( $0.06 < |M(\pi^+\pi^-) - 0.497| < 0.08$  GeV/c<sup>2</sup>).

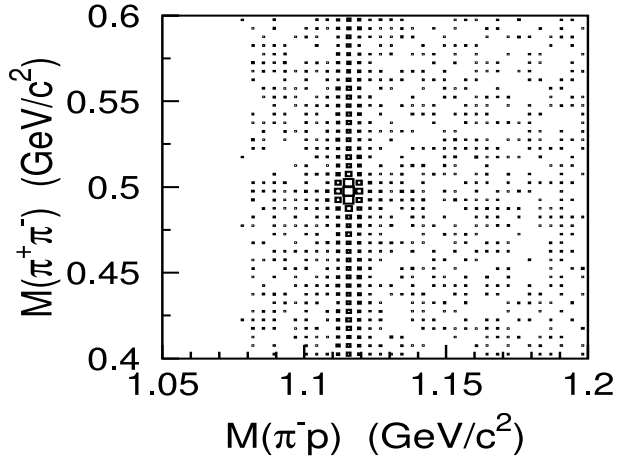


Figure 3. Scatter plot of  $m_{\bar{p}\pi^+}$  versus  $m_{\pi^+\pi^-}$  for  $J/\psi \rightarrow nK_S^0\bar{\Lambda}$  candidate events satisfying  $\chi_{1C}^2 < 5$  and  $L_{xy}(\Lambda) > 5$  mm.

of charged tracks for events satisfying these requirements plus  $L_{xy}(\Lambda) > 5$  mm is shown in Fig. 5, and a very clean neutron peak is seen. A fit with a Gaussian function yields a mass value consistent with that of the neutron. The  $\pi^+\pi^-$  invariant mass spectrum is shown in Fig. 6, and a  $K_S^0$  signal is clearly seen.

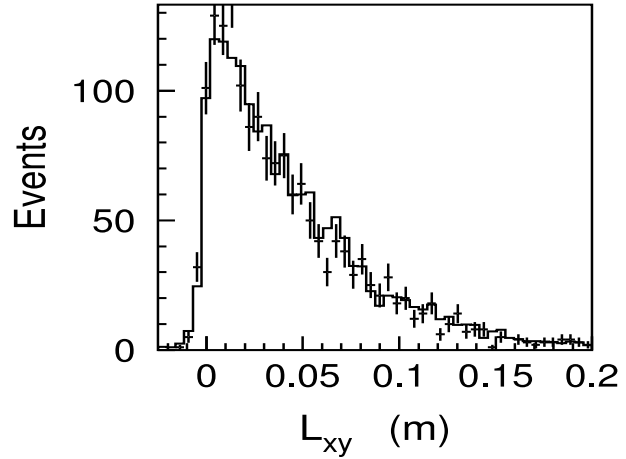


Figure 4. The  $\Lambda(\bar{\Lambda})$  decay length distributions with the  $\Lambda(\bar{\Lambda})$  and  $K_S^0$  mass selection requirements and  $\chi_{1C}^2 < 5$  for data and MC. The histogram is the sum of signal MC and background from  $K_S^0$  sidebands, and the crosses are data.

Backgrounds for  $J/\psi \rightarrow nK_S^0\bar{\Lambda}$  which contribute to the peak in the  $K_S^0$  signal region mainly come from  $J/\psi \rightarrow nK_S^0\bar{\Sigma}^0$  and  $J/\psi \rightarrow pK_S^0\bar{\Sigma}^-$  that survive selection criteria. Normalizing with the corresponding branching fractions and the number of  $J/\psi$  events in the data sample, a total of  $42 \pm 8$   $J/\psi \rightarrow nK_S^0\bar{\Sigma}^0$  and  $12 \pm 3$   $J/\psi \rightarrow pK_S^0\bar{\Sigma}^-$  background events are estimated. These events will be subtracted in determining the final branching fractions. Other surviving background events mainly come from  $J/\psi \rightarrow \bar{\Lambda}\Sigma^-\pi^+$ ,  $\bar{\Lambda}\Sigma^+\pi^-$ ,  $\Sigma^+\bar{\Sigma}^-(1385)$ , and  $\Sigma^-\bar{\Sigma}^+(1385)$ , and their charge conjugate channels, but they only give a flat contribution in the  $K_S^0$  signal region.

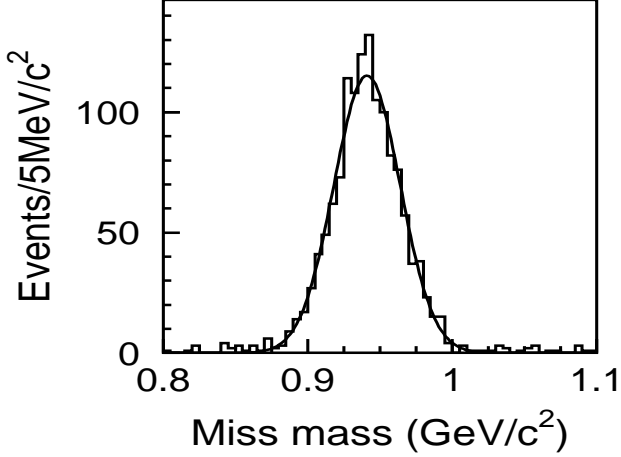


Figure 5. The missing mass spectrum of charged tracks in  $J/\psi \rightarrow nK_S^0\bar{\Lambda} + c.c.$  for events satisfying the requirements in Fig. 4 and  $L_{xy}(\Lambda) > 5$  mm.

The sum of these backgrounds, normalized by their branching fractions, is shown as the cross-hatched area in Fig. 6, and it is consistent with the background under the peak for data.

Using a Gaussian to describe the  $K_S^0$  and a second order polynomial function to model the background shape, a fit to the  $m_{\pi^+\pi^-}$  distribution is performed, shown as the curve in Fig. 6. A total of  $1058 \pm 33$   $K_S^0$  events are obtained. No  $K_S^0$  signal is observed in the  $m_{\pi^+\pi^-}$  invariant mass distribution for events which recoil against the  $\bar{\Lambda}$  sideband region ( $1.140 < m_{p\pi} < 1.164$   $\text{GeV}/c^2$ ). The detection efficiency for the signal is 6.09%, which is determined from a uniform phase space MC simulation. The branching fraction is:

$$\begin{aligned} & B(J/\psi \rightarrow nK_S^0\bar{\Lambda} + c.c.) \\ &= \frac{N_{obs} - N_{bg}}{N_{J/\psi} \cdot \epsilon \cdot B(\bar{\Lambda} \rightarrow \bar{p}\pi^+) \cdot B(K_S^0 \rightarrow \pi^+\pi^-)} \\ &= (6.46 \pm 0.20) \times 10^{-4}, \end{aligned}$$

where  $N_{obs}$  is the number of events observed ( $1058 \pm 33$ );  $N_{bg}$  is the number of background events from  $J/\psi \rightarrow nK_S^0\bar{\Sigma}^0$  ( $42 \pm 8$ ) and  $pK_S^0\bar{\Sigma}^-$  ( $12 \pm 3$ );  $\epsilon$  is the detection efficiency;  $N_{J/\psi}$  is

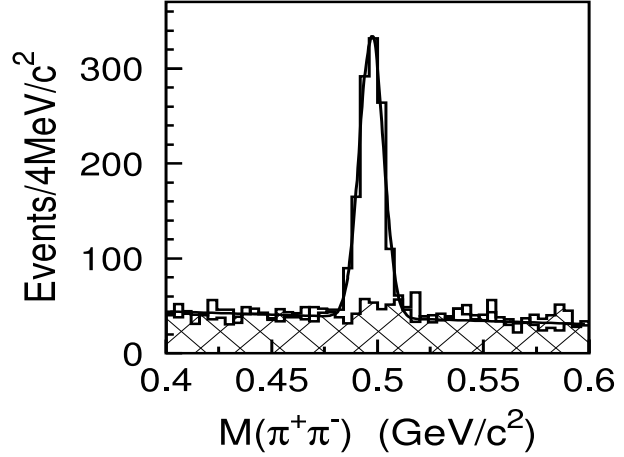


Figure 6. The  $\pi^+\pi^-$  invariant mass distribution for  $J/\psi \rightarrow nK_S^0\bar{\Lambda} + c.c.$  candidates satisfying the  $\Lambda(\bar{\Lambda})$  mass selection requirements,  $\chi_{1C}^2 < 5$ , and  $L_{xy}(\Lambda) > 5$  mm. The fit is also shown. The cross-hatched area is the sum of the backgrounds after normalization, as described in the text.

the number of  $J/\psi$  events; and  $B(\bar{\Lambda} \rightarrow \bar{p}\pi^+)$  and  $B(K_S^0 \rightarrow \pi^+\pi^-)$  are the branching fractions of  $\bar{\Lambda} \rightarrow \bar{p}\pi^+$  and  $K_S^0 \rightarrow \pi^+\pi^-$  [6]. The error is statistical only.

If we fit the charge conjugate channels separately, we obtain  $502 \pm 22$  events with an efficiency of 6.02% for  $J/\psi \rightarrow nK_S^0\bar{\Lambda}$ ,  $560 \pm 24$  events, an efficiency of 6.16% for  $J/\psi \rightarrow \bar{n}K_S^0\Lambda$ , and the following branching fractions:

$$\begin{aligned} B(J/\psi \rightarrow nK_S^0\bar{\Lambda}) &= (3.09 \pm 0.14) \times 10^{-4}, \\ B(J/\psi \rightarrow \bar{n}K_S^0\Lambda) &= (3.39 \pm 0.15) \times 10^{-4}, \end{aligned}$$

where the errors are statistical only. These results are consistent with each other in  $1.5\sigma$ .

In order to obtain a clean sample of  $J/\psi \rightarrow nK_S^0\bar{\Lambda}$  and  $\bar{n}K_S^0\Lambda$ , we require events to satisfy the  $\Lambda(\bar{\Lambda})$  and  $K_S^0$  mass selection requirements,  $\chi_{1C}^2 < 5$ , and  $L_{xy}(\Lambda) > 5$  mm, and also require the  $K_S^0$  decay length  $L_{xy}(K_S^0) > 5$  mm to eliminate backgrounds without a  $K_S^0$  in the final state, such as  $J/\psi \rightarrow \bar{\Lambda}\Sigma^-\pi^+$ . After this final selection, the background contribution is estimated to be less than 5%. Figure 7 shows the scatter plot of

$m_{\pi^-p}$  versus  $m_{\pi^+\pi^-}$  for  $J/\psi \rightarrow nK_S^0\bar{\Lambda}$  candidate events for all but the  $\Lambda(\bar{\Lambda})$  and  $K_S^0$  mass selection requirements, where the boxes in the plot show the signal and sideband regions. The invariant mass spectra of  $\Lambda K_S^0$ ,  $nK_S^0$ , and  $\bar{\Lambda}n(\Lambda\bar{n})$ , as well as the Dalitz plot for all selection requirements are shown in Fig. 8. In the  $\Lambda K_S^0$  invariant mass spectrum, an enhancement near  $\Lambda K_S^0$  threshold is evident, as is found in the  $\Lambda K$  mass spectrum in  $J/\psi \rightarrow pK^-\bar{\Lambda}$  [12]. If the enhancement is fitted with an acceptance weighted S-wave Breit-Wigner function and a function  $f_{bg}(\delta)$  describing the phase space “background” contribution, the fit leads to  $M=1.648\pm 0.006\text{GeV}/c^2$  and  $\Gamma = 61 \pm 21\text{MeV}/c^2$ , respectively. Here the errors are only statistical. The systematic uncertainties are not included since more accurate measurements of the mass and width should come from a full PWA involving interferences among  $N^*$  and  $\Lambda^*$  states. The fitted mass and width are consistent with those obtained from a partial wave analysis of  $J/\psi \rightarrow pK^-\bar{\Lambda}$  [12]. The  $X(2075)$  signal which was seen in the  $p\bar{\Lambda}$  invariant mass spectrum in  $J/\psi \rightarrow pK^-\bar{\Lambda}$  is not significant here. Using a Bayesian approach [13] and fixing the mass and width of  $X(2075)$  to 2075 MeV/ $c^2$  and 90 MeV/ $c^2$  respectively, the upper limit on the number of events observed  $N_{obs}^{UL}$  is 54 events at the 90% C.L.

The  $N^*$  state at around 1.9 GeV/ $c^2$  in the  $\Lambda K_S^0$  invariant mass spectrum and the  $\Lambda^*$  states at around 1.5 and 1.7 GeV/ $c^2$  in the  $nK_S^0$  invariant mass spectrum are present. A larger data sample and a partial wave analysis are needed to analyze these  $N^*$  and  $\Lambda^*$  states.

### 3.2. Measurement of $\psi(2S) \rightarrow nK_S^0\bar{\Lambda} + c.c.$

Using the same criteria as in Section 3.1, we select  $\psi(2S) \rightarrow nK_S^0\bar{\Lambda} + c.c.$  events from the BES-II sample of 14M  $\psi(2S)$  events. The  $\pi^-p$  and  $\pi^+\pi^-$  invariant mass spectra, the scatter plot of  $m_{\pi^-p}$  versus  $m_{\pi^+\pi^-}$ , and the missing mass spectrum after the final selection are shown in Fig. 9. The  $\Lambda$  and  $K_S^0$  signals are obvious.

Fitting the  $\pi^+\pi^-$  mass spectrum with a Gaussian for the  $K_S^0$  signal and a first order polynomial background, as shown in Fig. 10, yields  $50 \pm 7 K_S^0$

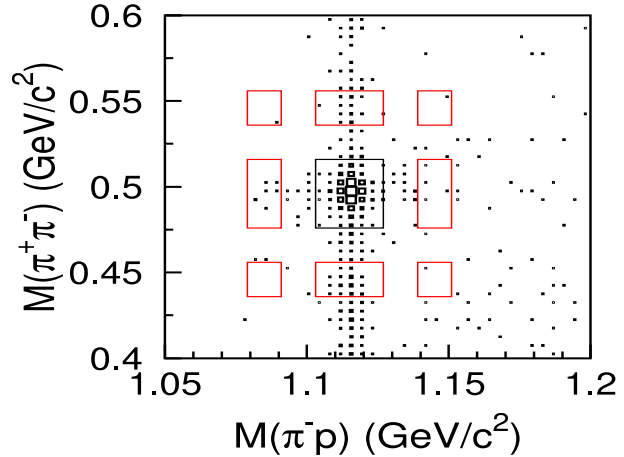


Figure 7. The scatter plot of  $m_{\pi^-p}$  versus  $m_{\pi^+\pi^-}$  for  $J/\psi \rightarrow nK_S^0\bar{\Lambda}$  candidates after all selection requirements except for the  $\Lambda$  and  $K_S^0$  mass requirements. The boxes in the plot show the signal and sideband regions.

events. The statistical significance of the  $K_S^0$  is about  $7.2\sigma$ . The  $2 \pm 1$  background events from the  $\Lambda(\bar{\Lambda})$  sidebands and  $2 \pm 1$  background events from  $\psi(2S) \rightarrow nK_S^0\bar{\Sigma}^0$  are subtracted. A uniform phase space MC simulation determines the detection efficiency to be 9.16%. The corresponding branching fraction is:

$$B(\psi(2S) \rightarrow nK_S^0\bar{\Lambda} + c.c.) = (8.11 \pm 1.14) \times 10^{-5}.$$

Here the error is statistical only.

### 3.3. Systematic Errors

In this analysis, the systematic errors on the branching fractions mainly come from following sources.

#### 3.3.1. MDC tracking

The MDC tracking efficiency has been measured using channels like  $J/\psi \rightarrow \rho\pi$ ,  $\Lambda\bar{\Lambda}$ , and  $\psi(2S) \rightarrow \pi^+\pi^-J/\psi$ ,  $J/\psi \rightarrow \mu^+\mu^-$ . The MC simulation agrees with data within 1 to 2% for each charged track [11]. Thus 8% is taken as the systematic error coming from MDC tracking for the

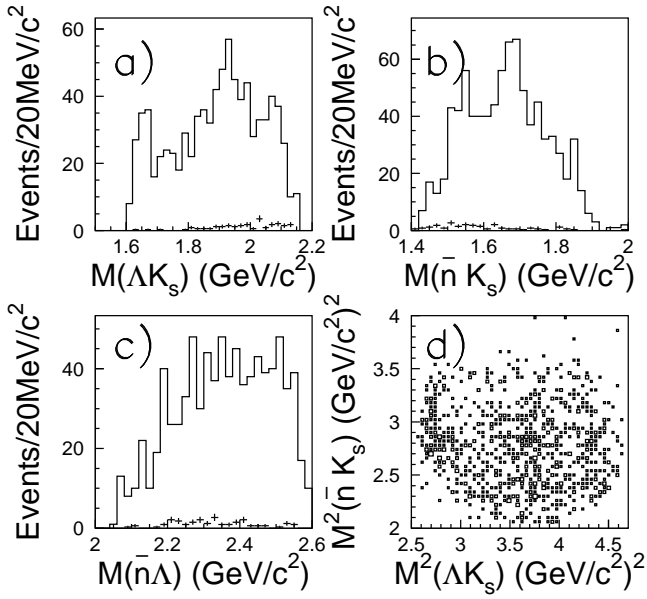


Figure 8. The invariant mass spectra of (a)  $\Lambda K_S^0$ , (b)  $\bar{n}K_S^0$ , and (c)  $\bar{n}\Lambda$ , as well as (d) the Dalitz plot for candidate events after all selection criteria. The crosses show the sideband backgrounds.

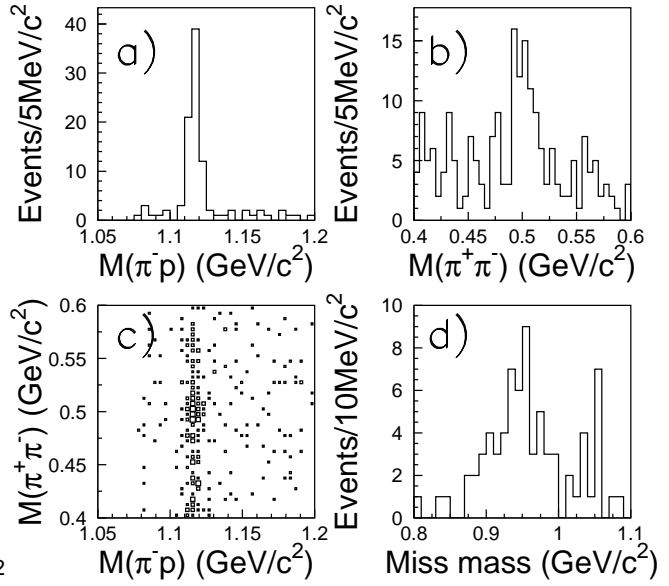


Figure 9. The invariant mass spectra of (a)  $\pi^- p$  and (b)  $\pi^+ \pi^-$ , (c) the scatter plot of  $M_{\pi^- p}$  versus  $M_{\pi^+ \pi^-}$ , and (d) the missing mass spectrum for events satisfying the  $\Lambda(\bar{\Lambda})$  mass selection requirement,  $\chi_{1C}^2 < 5$ , and  $L_{xy}(\Lambda) > 5$  mm.

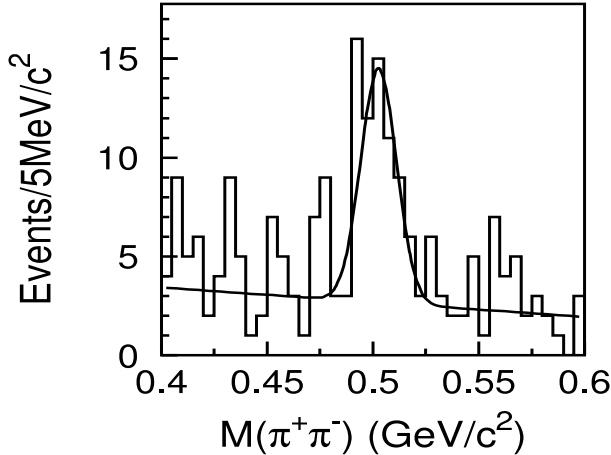


Figure 10. The fit of  $\pi^+\pi^-$  invariant mass spectrum for  $\psi(2S) \rightarrow nK_S^0\bar{\Lambda} + c.c.$  for events satisfying the requirements in Fig. 9d.

4-prong events considered in this analysis.

### 3.3.2. Kinematic fit

The systematic error from the 1C kinematic fit should be smaller than that from the 4C kinematic fit, since there are fewer constraints. Various studies show that the uncertainty of the 4C kinematic fit is around 4% [14]. Here we conservatively take 4% as the error from the 1C kinematic fit.

### 3.3.3. Particle identification

In Ref. [11], the particle identification efficiency of  $\pi$ ,  $K$ , and  $p$  are analyzed in detail. Here, only one charged track is required to be identified as a  $p$  or  $\bar{p}$ , and the systematic error from particle identification is less than 2%.

### 3.3.4. $\Lambda$ and $K_S^0$ vertex finding

In Ref. [15],  $J/\psi \rightarrow \Lambda\bar{\Lambda} \rightarrow \pi^+\pi^-p\bar{p}$  is chosen as the reference channel to study the systematic error of the  $\Lambda$  vertex finding algorithm, and 1.2% is determined as the systematic error for one  $\Lambda$  vertex. For  $K_S^0$ , the efficiency of the secondary vertex finding is studied using  $J/\psi \rightarrow K^*(892)\bar{K} + c.c.$  events, and the systematic error is about 4.1% [16].

### 3.3.5. MC model

Different hadronization models for simulating the hadronic interactions give different detection efficiencies. Their differences are taken as systematic errors. The systematic errors are 7.0% and 14.7% for  $J/\psi \rightarrow nK_S^0\bar{\Lambda}$  and its conjugate channel, respectively, and 11.1% for  $\psi(2S) \rightarrow nK_S^0\bar{\Lambda} + c.c.$ . The efficiency differences with or without considering the intermediate  $N^*$  and  $\Lambda^*$  states are also taken as the systematic errors. They are 5.3% and 4.5% for  $J/\psi \rightarrow nK_S^0\bar{\Lambda}$  and  $J/\psi \rightarrow \bar{n}K_S^0\Lambda$ , respectively.

### 3.3.6. Background uncertainty

The background uncertainties come from the uncertainties associated with the estimation of the sideband backgrounds, continuum events, and the events from other background channels, as well as the uncertainties of the background shape, different fit ranges, etc. Therefore, the statistical errors in the estimated background events, the largest difference in changing the background shape, and the difference of changing the fit ranges are taken as the systematic errors for the background uncertainty.

### 3.3.7. Intermediate decay branching fractions

The branching fractions of  $\Lambda \rightarrow p\pi^-$  and the  $K_S^0 \rightarrow \pi^+\pi^-$  decays are taken from the PDG [6]. The errors on these branching fractions are taken as systematic errors in our measurements.

### 3.3.8. Number of $J/\psi$ and $\psi(2S)$ events

The total number of  $J/\psi$  events is  $(57.70 \pm 2.62) \times 10^6$ , determined from inclusive 4-prong hadrons [17], and the total number of  $\psi(2S)$  events  $N_{\psi(2S)}$  is  $(14.0 \pm 0.6) \times 10^6$ , determined from inclusive hadronic events [18]. The uncertainty on the number of  $J/\psi$  events, 4.7%, and the uncertainty on the number of  $\psi(2S)$  events, 4.0%, are also systematic errors.

The above systematic errors are all listed in Table 1. The total systematic error is determined by adding all terms in quadrature.

#### 4. Results

The decays of  $J/\psi$  and  $\psi(2S)$  to  $nK_S^0\bar{\Lambda} + c.c.$  are observed for the first time, and their branching fractions are:

$$\begin{aligned} B(J/\psi \rightarrow nK_S^0\bar{\Lambda} + c.c.) &= \\ &(6.46 \pm 0.20 \pm 1.07) \times 10^{-4}, \\ B(J/\psi \rightarrow nK_S^0\bar{\Lambda}) &= (3.09 \pm 0.14 \pm 0.58) \times 10^{-4}, \\ B(J/\psi \rightarrow \bar{n}K_S^0\Lambda) &= (3.39 \pm 0.15 \pm 0.48) \times 10^{-4}, \\ B(\psi(2S) \rightarrow nK_S^0\bar{\Lambda} + c.c.) &= \\ &(0.81 \pm 0.11 \pm 0.14) \times 10^{-4}. \end{aligned}$$

The ratio of the branching fractions of  $\psi(2S)$  and  $J/\psi$  decaying to  $nK_S^0\bar{\Lambda} + c.c.$  is  $Q_h = (12.6 \pm 3.5)\%$  and obeys the 12% rule well.

There is no obvious enhancement near  $n\bar{\Lambda}$  threshold. The upper limit on the branching fraction on the near-threshold enhancement  $X(2075)$  at  $n\bar{\Lambda}$  threshold at the 90 % C.L. is:

$$\begin{aligned} &B(J/\psi \rightarrow K_S^0 X) \cdot B(X \rightarrow n\bar{\Lambda} + c.c.) \\ = &\frac{N_{obs}^{UL}}{N_{J/\psi} \cdot \epsilon \cdot B(\Lambda \rightarrow p\pi^-) \cdot B(K_S^0 \rightarrow \pi^+\pi^-) \cdot (1 - \delta_{sys})} \\ &< 4.9 \times 10^{-5} \text{ (90\% C.L.)}, \end{aligned}$$

where  $N_{obs}^{UL}$  is 54 events;  $\epsilon=5.32\%$  is the detection efficiency considering the angular distributions;  $N_{J/\psi}$  is the number of  $J/\psi$  events;  $B(\Lambda \rightarrow p\pi^-)$  and  $B(K_S^0 \rightarrow \pi^+\pi^-)$  are the  $\Lambda \rightarrow p\pi^-$  and  $K_S^0 \rightarrow \pi^+\pi^-$  branching fractions, and  $\delta_{sys}$  is the systematic error (17.3%). Taking into account the isospin factor, the branching fraction upper limit for  $B(J/\psi \rightarrow K_S^0 X) \cdot B(X \rightarrow n\bar{\Lambda} + c.c.)$  is not inconsistent with that for  $B(J/\psi \rightarrow KX) \cdot B(X \rightarrow p\bar{\Lambda} + c.c.)$  [4].

#### 5. Acknowledgments

The BES collaboration thanks the staff of BEPC and computing center for their hard efforts. This work is supported in part by the National Natural Science Foundation of China under contracts Nos. 10491300, 10225524, 10225525, 10425523, 10625524, 10521003, the Chinese Academy of Sciences under contract No. KJ 95T-03, the 100 Talents Program of CAS under Contract Nos. U-11, U-24, U-25, and the Knowledge Innovation Project of CAS under

Contract Nos. U-602, U-34 (IHEP), the National Natural Science Foundation of China under Contract No. 10225522 (Tsinghua University), and the Department of Energy under Contract No. DE-FG02-04ER41291 (U. Hawaii).

#### REFERENCES

1. J. J. Aubert, *et al.*, Phys. Rev. Lett. **33**,1404 (1974).
2. J. E. Augustin, *et al.*, Phys. Rev. Lett. **33**,1406 (1974).
3. L. Köpke and A. Wermes, Phys. Rep. **174**, 67 (1989).
4. BES Collaboration, M. Ablikim *et al.*, Phys. Rev. Lett. **93**, 112002 (2004).
5. T. Appelquist and H. D. Politzer, Phys. Rev. Lett. **34**, 43 (1975); A. De Rujula and S. L. Glashow, *ibid*, page 46.
6. W.-M. Yao *et al.* (Particle Data Group), J. Phys. G **33**,1 (2006).
7. P. B Mackenzie, G. P. Lepage, Phys. Rev. Lett. **47**, 1244 (1981).
8. W. S. Hou and A. Soni, Phys. Rev. Lett. **50**, 569 (1983).
9. W. S. Hou, Phys. Rev. D **55**, 6952 (1992).
10. BES Collaboration, J. Z. Bai *et al.*, Nucl. Instrum. and Methods A **458**, 627 (2001).
11. BES Collaboration, M. Ablikim *et al.*, Nucl. Instrum. and Methods A **552**, 344 (2005).
12. H. X. Yang for BES Collaboration, Int. J. Mod. Phys. A **20**, 1985 (2005).
13. G. J Feldman and R. D. Cousins, Phys. Rev. D **57**,3873 (1998).
14. BES Collaboration, M. Ablikim *et al.*, Phys. Rev. D **74**, 012004 (2006).
15. BES Collaboration, M. Ablikim *et al.*, Phys. Lett. B **648**, 149 (2007).
16. BES Collaboration, M. Ablikim *et al.*, Phys. Rev. Lett. **92**, 052001 (2004).
17. S. S. Fang *et al.*, HEP&NP **27**, 277 (2003) (in Chinese).
18. X. H. Mo *et al.*, HEP&NP, **28**, 455 (2004).

Table 1  
Summary of the systematic errors.

Sources	Relative Error (%)			
	$J/\psi \rightarrow nK_S^0\Lambda$	$J/\psi \rightarrow \bar{n}K_S^0\Lambda$	$J/\psi \rightarrow X(2075)K_S^0$	$\psi(2S) \rightarrow nK_S^0\Lambda + c.c.$
decay modes				
MDC tracking	8.0	8.0	8.0	8.0
Kinematic fit	4.0	4.0	4.0	4.0
Particle ID	2.0	2.0	2.0	2.0
MC model	15.6	8.3	9.4	11.1
Background uncertainty	2.1	5.1	9.3	7.1
$\Lambda$ and $K_S^0$ reconstruction	1.2	1.2	4.3	1.2
Intermediate decay branching fractions	0.9	0.9	0.9	0.9
Numbers of $J/\psi$ and $\psi(2S)$ events	4.7	4.7	4.7	4.0
Total systematic error	18.9	14.3	17.3	16.6